The Response of Ice Shelf Basal Melting to Variations in Ocean Temperature

PAUL R. HOLLAND AND ADRIAN JENKINS

British Antarctic Survey, Cambridge, United Kingdom

DAVID M. HOLLAND

Courant Institute of Mathematical Sciences, New York University, New York, New York

(Manuscript received 21 February 2007, in final form 23 October 2007)

ABSTRACT

A three-dimensional ocean general circulation model is used to study the response of idealized ice shelves to a series of ocean-warming scenarios. The model predicts that the total ice shelf basal melt increases quadratically as the ocean offshore of the ice front warms. This occurs because the melt rate is proportional to the product of ocean flow speed and temperature in the mixed layer directly beneath the ice shelf, both of which are found to increase linearly with ocean warming. The behavior of this complex primitive equation model can be described surprisingly well with recourse to an idealized reduced system of equations, and it is shown that this system supports a melt rate response to warming that is generally quadratic in nature. This study confirms and unifies several previous examinations of the relation between melt rate and ocean temperature but disagrees with other results, particularly the claim that a single melt rate sensitivity to warming is universally valid. The hypothesized warming does not necessarily require a heat input to the ocean, as warmer waters (or larger volumes of "warm" water) may reach ice shelves purely through a shift in ocean circulation. Since ice shelves link the Antarctic Ice Sheet to the climate of the Southern Ocean, this finding of an above-linear rise in ice shelf mass loss as the ocean steadily warms is of significant importance to understanding ice sheet evolution and sea level rise.

1. Introduction

Ice shelves provide an important interface between the Antarctic Ice Sheet and surrounding ocean. Approximately 80% of Antarctic ice passes through ice shelves before being lost through melting and iceberg calving (Jacobs et al. 1992), and a link appears to exist between the characteristics and extent of ice shelves and the dynamics of the ice streams that feed them (e.g., Scambos et al. 2000; Rignot et al. 2004). This means that the mass balances of individual ice shelves are of great importance to the evolution of the Antarctic Ice Sheet as a whole and are therefore crucial to our understanding of sea level rise. In addition, interaction between ice shelves and ocean water leads to the formation of Antarctic Bottom Water, a key component of the global thermohaline circulation (Orsi et al. 1999).

Recent satellite observations of the Antarctic Ice Sheet fringing the Amundsen Sea have confirmed that various ice streams there are thinning (Wingham et al. 2006), accelerating (Joughin et al. 2003), and experiencing retreat of their associated grounding lines, at which the ice stream goes afloat (Rignot 1998). These processes lead to a transfer of mass from the ice sheet to the oceans, though it is unclear whether Antarctica as a whole has a negative mass balance at present (Rignot and Thomas 2002; Zwally et al. 2005; Wingham et al. 2006). The ice streams observed to be thinning are glaciologically distinct, but all share similar behavior, leading to suspicion that the thinning results from a common change in external forcing rather than internal glacier dynamics. Observed thinning of the ice shelves at the termini of these ice streams (Shepherd et al. 2004) has led several researchers to suggest that an increase in ice shelf basal melting, caused by warmer ocean waters reaching these ice shelves, is the ultimate driver of the inland changes. Limitations in our understanding of these processes present a fundamental barrier to accurate predictions of sea level rise (Lemke et al. 2007).

Corresponding author address: Dr. Paul R. Holland, British Antarctic Survey, High Cross, Madingley Road, Cambridge CB3 0ET, United Kingdom.
E-mail: p.holland@bas.ac.uk

DOI: 10.1175/2007JCLI1909.1

Over recent years observations and modeling studies have built up a consistent picture of the interactions between ice shelves and oceans. Under the larger ice shelves such as Filchner–Ronne and Ross, cold and dense high-salinity shelf water (HSSW) intrudes into the cavity after being generated by brine rejection from sea ice formation on the continental shelf offshore of the ice front (Nicholls and Østerhus 2004). As a consequence of the decrease in seawater's freezing temperature with increasing pressure, this HSSW (which is at the surface freezing temperature) has heat available to melt the deeper parts of the ice shelf, releasing fresh, cold meltwater at depth. Conversely, as the meltwater rises the increasing in situ freezing temperature causes it to become supercooled, form frazil ice, and freeze onto the base of the ice shelf (Jenkins and Bombosch 1995; Holland and Feltham 2006). In contrast to this picture, the smaller ice shelves surrounding the Amundsen and Bellingshausen Seas are impacted directly by Circumpolar Deep Water (CDW) upwelling from the deep ocean offshore of the continental shelf break (Jacobs et al. 1996). These ice shelves have a simpler regime in which the ice shelf base melts everywhere (Payne et al. 2007).

There is a reasonable volume of data showing that the Southern Ocean has warmed over the last 50 yr, but the relevance of this warming to the melting of ice shelves is uncertain owing to a shortage of oceanographic data in the inaccessible southernmost regions. The positive heat content trend reported by Levitus et al. (2000, 2005) centers on the sea surface at 40°S and extends to 1100-m depth, while Gille (2002) found a larger warming trend at 700–1100-m depth. We are not aware of any studies showing a robust circumpolar trend south of 65°S or much deeper than 1000 m, so it has not yet been demonstrated that the CDW apparently responsible for ice shelf thinning in the Amundsen Sea sector has persistently warmed as a water mass. CDW upwells around Antarctica after residing at great depth for many years, so it is not necessarily affected by atmospheric warming on short (decadal or less) time scales. The HSSW intruding beneath the largest ice shelves cannot warm significantly because its properties are fixed by brine rejection at the surface freezing point (MacAyeal 1984), but a general warming of HSSW source areas might reduce its rate of production.

The temperature of waters in contact with an ice shelf base could be altered by changes in ocean dynamics rather than water mass properties. Jacobs (2006) postulates that variation in the southern annular mode (SAM; the primary mode of atmospheric variability in the Southern Hemisphere) could affect CDW flooding of Antarctic continental shelves; the growing strength of midlatitude westerlies associated with the increasingly positive SAM index (Marshall et al. 2004) could increase northward Ekman drift in the ocean, promoting divergence-induced upwelling of CDW near Antarctica. Whether this translates into a larger flux of CDW onto the continental shelf and increased ice shelf melting is another matter.

The aim of this modeling study is to step back from detailed studies of the effect of oceanographic change in specific locations and instead assess the broad response of ice shelf basal melting to the presence of seawater at a range of temperatures offshore of the ice front. This can be viewed as either a generalization of different similarly shaped ice shelves experiencing a variety of ocean temperatures, or as a study of the impact of warming or cooling of the ocean offshore of a particular ice shelf. We generalize this study as far as possible by adopting an idealized ice shelf topography, seabed bathymetry, and ocean forcing, but we ensure that the governing equations and basal melting formulation that we use contain as full an expression of the relevant physics as possible. Our goal is a wider understanding of the relationship between ocean heat content and ice shelf basal melting rates over the full range of relevant seawater temperatures.

The paper proceeds as follows: in section 2 we discuss previous studies relevant to the response of ice shelf basal melting to ocean warming; in section 3 we describe the model that we used to examine this response; in section 4 we discuss the detail of model results for illustrative cases in the default simulation class and present the results of the main warming study; in section 5 we assess the sensitivity of all results to variations in the sub–ice shelf cavity shape; and in sections 6 and 7 we discuss the conclusions of this study for the melting of ice shelves at present and in the future.

2. Previous studies

There are many experimental and theoretical studies of ice melting in saline water (Gade 1993), but most do not explicitly state a relation between the melt rate and water temperature. Of those that do, all report an above-linear increase in melt rate as the seawater warms. Assuming similarity between boundary layer measurements of heated plates in air and seawater in the meltwater plume offshore of a vertical glacier face, Greisman (1979) derived a formula relating the ice melt rate to seawater temperature raised to the power 1.4. Russell-Head (1980) performed experiments with model icebergs placed in a tank of seawater at temperatures between 0° and +20°C, finding that the melt rate varied according to a 1.5-power relation with tempera-

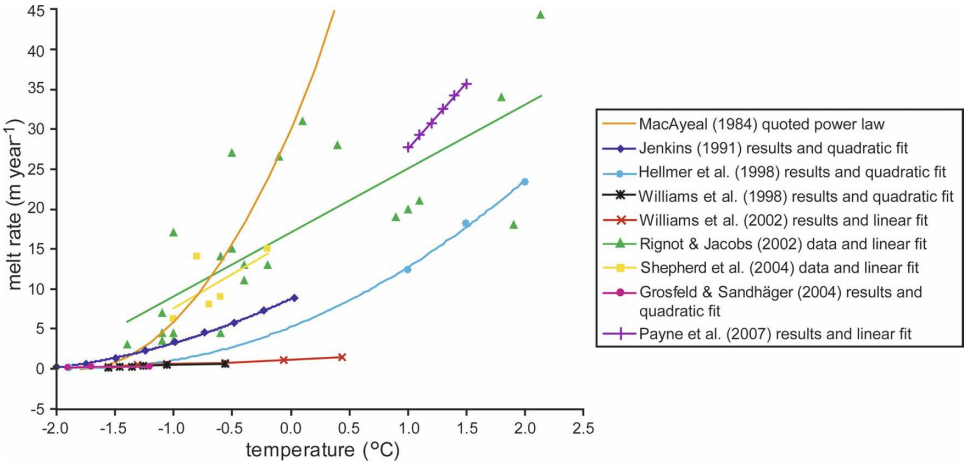

FIG. 1. Relationships between ice shelf melting and ocean temperature found by previous studies. Where necessary, a freezing temperature of −1.8°C is used to calculate the curves. The methods of each study are described in Table 1. Linear fits to the data of Rignot and Jacobs (2002) and Shepherd et al. (2004) are based entirely on the data points shown here. All fits to model results are linear unless a quadratic curve explained a significant fraction more of the variance (see legend).

ture, which is broadly supported by iceberg observations (Budd et al. 1980; Hamley and Budd 1986). Josberger and Martin (1981) experimented with a model ice wall melted by seawater, finding that a 1.6-power relation was valid for temperatures between −0.1° and +9°C. Gebhart et al. (1983) present results indicating that similar relations are applicable to several other experimental studies.

We now describe the results from all studies that we are aware of that examine the relationship between (specifically) ice shelf basal melting and ocean temperature. Figure 1 shows these results (described in Table 1), but should be viewed with caution because a range of different assumptions, investigative approaches, and warming scenarios were used; in particular, results from different modeling studies should not be intercompared. Unsurprisingly, all studies concur that the spatially averaged net basal melting of an ice shelf (melting minus refreezing, where appropriate) rises when the ocean temperature offshore of the ice front increases. However, the studies are not in agreement on the nature of this rise, with some finding that it is approximately linear and others above linear. We now review the relevant literature.

MacAyeal (1984) formulated a simple two-layer model of ocean dynamics beneath an ice shelf in which an inflowing saline deep layer is compensated by an overlying fresh meltwater outflow. The flow speed in both layers is proportional to the temperature difference between the deep layer and the ice shelf base (a proxy for the density difference between layers) and melting is proportional to the product of this speed and the temperature difference. Overall, this leads to a power 2 relation between melt rate and deep-water temperature.

Rignot and Jacobs (2002) used satellite observations of ice shelf surface height and flow to infer the average equilibrium melt rates of all major Antarctic ice shelves

TABLE 1. Description of the studies referred to in Fig. 1.

Reference	Ice shelves	Description
MacAyeal (1984)	Idealized	Theoretical relation for melting by a two-layer ocean
Jenkins (1991)	Idealized	One-dimensional modeling of ice shelf meltwater plume
Hellmer et al. (1998)	Pine Island	Two-dimensional vertical section modeling of sub–ice shelf ocean cavity
Williams et al. (1998, 2002)	Amery	Three-dimensional numerical modeling of sub–ice shelf ocean cavity
Rignot and Jacobs (2002)	All	Satellite interferometry and altimetry of ice shelves combined with nearby oceanographic data
Shepherd et al. (2004)	Amundsen sector	Repeated satellite altimetry and data of Rignot and Jacobs (2002) and Giulivi and Jacobs (1997)
Grosfeld and Sandhäger (2004)	Idealized	Coupled modeling of two-dimensional ice shelf and three-dimensional ocean
Payne et al. (2007)	Pine Island	Two-dimensional horizontal section modeling of ice shelf meltwater plume

within "one glacier width" of the grounding line. Disregarding Smith Glacier and adding a data point at the origin, they plotted a linear fit between these melt rates and the difference between the nearest ocean temperature measurement and the seawater freezing point at 88% of the appropriate grounding line ice thickness. These data for ice shelves in the Amundsen Sea sector were scaled up to whole-shelf values (using a melt profile from Pine Island Glacier) by Shepherd et al. (2004) and then modified according to their observations of ice shelf thinning rates. Curves were drawn suggesting a linear relation between these data and the nearest temperature above freezing from the oceanographic data of Giulivi and Jacobs (1997); the depths of those temperatures are not stated, but the values are different to those used by Rignot and Jacobs (2002). It is unclear what temperature should be used for such a relation considering the lack of appropriate data, variation in circulation and topography between ice shelves, and spatial and temporal oceanic variability. Both studies employ melt rate data from near the grounding line, which could be problematic because altimetry of this area is subject to the most significant errors (Jenkins et al. 2006), the ice shelf is not necessarily freely floating, and surface velocities may not represent the depth average. The distance between measurements may also be large enough to miss spatial variability (e.g., compare Shepherd et al. 2004 and Payne et al. 2007).

There are many (ocean) modeling studies of melting at the base of individual ice shelves, and a significant proportion of these contain studies of the sensitivity of the net melt rate to variation in ocean temperature. However, some of these studies are solely intended to reveal the response of the model to uncertainty in the ocean forcing (Jenkins 1991; Hellmer and Jacobs 1995; Grosfeld and Gerdes 1998; Smedsrud and Jenkins 2004); generally only one warming scenario is undertaken, precluding any attempt to derive a relationship between melt rate and warming. It would be inappropriate to intercompare these models because of the wide variety of different modeling strategies and warming scenarios involved. For that reason, the results are not plotted in Fig. 1.

To our knowledge, there are six modeling studies in which the sensitivity of the ice shelf basal melt rate to more than one change in ocean temperature is examined in a manner enabling a curve to be drawn between simulations. The most comprehensive are the studies of Williams et al. (1998, 2002), who examined the response of a three-dimensional model of the ocean beneath Amery Ice Shelf to a variety of warmings encompassing the temperature range −1.8° to +1.5°C. The model's net basal melt rate was found to increase linearly in response to warming (slightly below linearly in the case of Williams et al. 1998), but their modeling approach contains a number of potential flaws. The ice front forms the northern boundary of their model domain, so the barotropic flow into and out of the cavity is fixed throughout to values determined from present-day temperature and salinity conditions, neglecting any variations in exchange that may occur under warming scenarios. In addition, they used free-slip boundary conditions at the sea bed and ice shelf base (M. J. M. Williams 2006, personal communication), implying that their ocean flows are (unrealistically) predominantly geostrophic.

Jenkins (1991) used a one-dimensional model of meltwater plumes beneath an idealized ice shelf to investigate the response of the basal melt rate to warming of the deep water below. The deeper water is stagnant with fixed properties and enters the plume according to a simple entrainment relation. The response of the model melt rate to a variety of temperatures in the range −2° to 0°C is clearly above linear. Payne et al. (2007) applied an extended two-dimensional version of this plume model to a study of flow beneath Pine Island Glacier, setting the CDW forcing the model to salinities between 34.2 and 34.7 and temperatures between +1.0° and +1.5°C and finding a linear response to temperature over this relatively small range.

Hellmer et al. (1998) applied a two-dimensional vertical section ocean model to the cavity beneath Pine Island Glacier and tested the model's response to CDW temperatures of −1.88°, +1.0°, +1.5°, and +2.0°C. Though sparse, the results appear to imply an above-linear relation. The coupled (two-dimensional) ice shelf and (three-dimensional) ocean models of Grosfeld and Sandhäger (2004), representing an idealized version of Filchner–Ronne Ice Shelf, were subjected to two climate warming perturbations so that the study encompassed the range −1.9° to −1.5°C. The melt rate response was marginally below linear over the temperature ranges considered.

Finally, Walker and Holland (2007) applied coupled vertical section models of an ice shelf (one-dimensional) and ocean (two-dimensional) to an idealized domain reminiscent of Filchner Ice Shelf, forcing the system with a series of ice front ocean temperature profiles in the range −2.0° to −1.6°C. They found that the response of ice shelf melting to warming was initially above linear, but later became below linear as the ice shelf base was flattened to varying degrees by melting. The results are not completely steady, which complicates the comparison, and they speculate that in reality an unmodeled dynamic response of the ice stream feeding the ice shelf could maintain its basal slope and,

consequently, the nonlinear response to warming. For these reasons we do not include their results in Fig. 1.

As revealed by this discussion, no clear consensus has emerged about the functional response of basal melting to ocean warming over the full range of relevant temperatures. In the remainder of this paper, we investigate this issue by applying a complex ocean model to a simplified representation of the problem.

3. Modeling approach

a. Model setup

In this study we employ the three-dimensional isopycnic-coordinate ocean general circulation model (GCM) that was adapted to the study of sub-ice shelf cavities by Holland and Jenkins (2001). The model consists of 10 uniform-density (isopycnic) layers beneath a mixed layer of varying density that interacts with the overlying ice shelf or atmosphere. Deeper waters interact with the mixed layer according to an entrainment/detrainment algorithm that includes the turbulent kinetic energy generated by frictional stress at the ice shelf base, the buoyancy flux due to melting, and a parameterization of energy dissipation processes. The model's horizontal coordinates are longitude (x) and latitude (y), the model domain covers the area of 70°–80°S by 0°–10°E, and the grid resolution is 0.5° in longitude (9.7–19.1 km). Each simulation is run for 10 yr, after which the model is fully spun up, and all results presented are from the final steady state.

A range of different ice draft and bedrock topography profiles are considered, as shown in Fig. 2 and listed in Table 2. A set of warming experiments is performed on each cavity shape, so each topographic setup is referred to as a "simulation class" and each individual model run is referred to by simulation class with the ocean temperature as a subscript, for example, $A_{-1.8}$. Cavity shapes are uniform in the zonal (x) direction and fixed in time. Our basic simulation class (A) has a flat bedrock of 1100-m depth beneath an ice shelf 5° of latitude in length with draft B tapering linearly from 1000-m depth at the grounding line to 200-m depth at the ice front. This class provides the primary results of this study, while other cavity shapes are used solely to examine the sensitivity of the melt rate–ocean temperature relation. Other simulation classes use a smaller, steeper ice shelf (B and D), a nonlinear ice shelf profile (C and D), tapered sidewalls (E and F), and a sloping bedrock topography (G and H). The nonlinear ice shelf draft is calculated according to

$$B = \frac{-\alpha_1}{(\alpha_2 + y)^{1/4}}, \qquad (1)$$

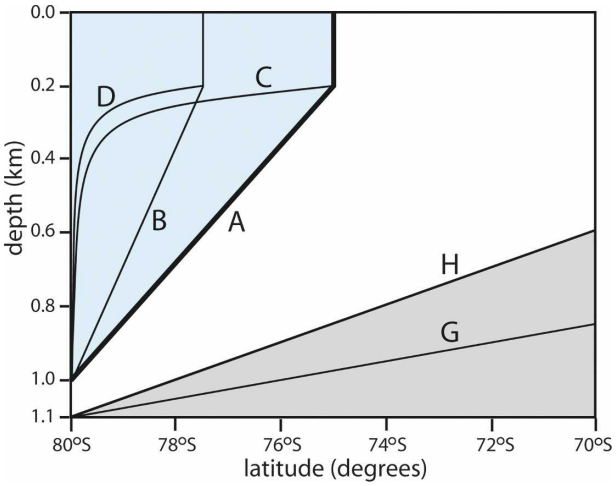

FIG. 2. Schematic of domain profiles for each simulation class (as labeled). The main class of simulations (A) uses the linear shelf profile shown by the thick line, while the sensitivity studies use domains shown by the thinner lines. The ice shelf profiles are all varied while keeping the bedrock flat and the seabed slopes are varied while the ice shelf is fixed to the linear A profile. Simulations E and F use the A profile, flat bedrock, and tapered lateral sidewalls.

where constants α_1 and α_2 are chosen to give the required values at the grounding line and ice front. This basal profile represents the limiting case of an ice shelf that is laterally confined but experiences negligible lateral drag, while the default linear profile represents the opposite limiting case of a confined ice shelf in which lateral drag supports all of the driving stress (van der Veen 1999). To represent ice shelf cavities that taper to a narrow grounding line (e.g., beneath Amery Ice Shelf), the east and west sidewalls in experiments E and F slope linearly inward such that the grounding line width is reduced to 50% and 10% (respectively) of the width of the northern boundary.

Solid no-slip walls surround the domain on all sides and no fluxes are permitted at the ocean surface. The

TABLE 2. Characteristics of the model simulation classes referred to in this paper. For each class a range of different thermal forcings are considered.

Simulation class	Ice shelf	Length	Bedrock relief
A	Linear	5°	None
B	Linear	2.5°	None
C	Nonlinear	5°	None
D	Nonlinear	2.5°	None
E	Linear	5°	50% width grounding line
F	Linear	5°	10% width grounding line
G	Linear	5°	250-m bedrock slope
H	Linear	5°	500-m bedrock slope

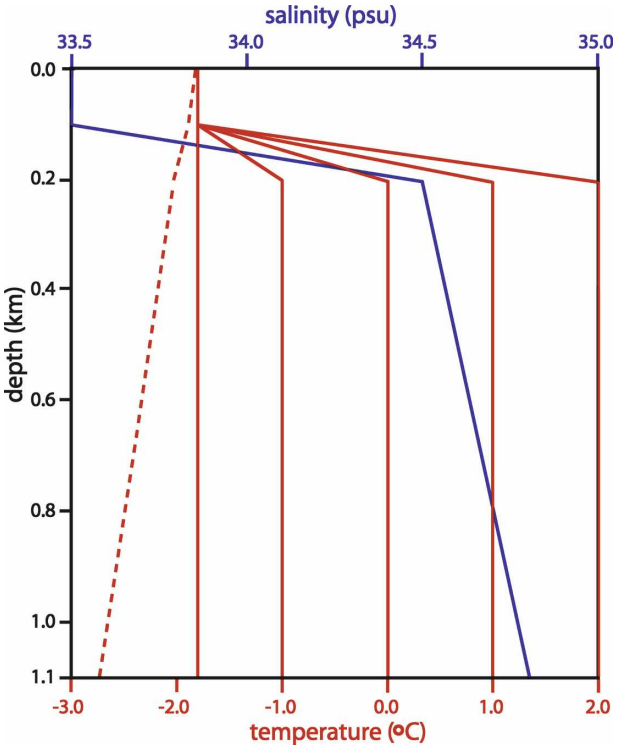

FIG. 3. Idealized seawater properties used to force the model on the northern boundary (solid lines). The salinity profile is used throughout all simulations, while the temperature profile varies for each simulation in a class (some sample temperature profiles are shown). The dashed line is the freezing temperature at the salinity and depth shown.

only forcing of the model ocean is applied on the northern boundary, where there is a 5-cell-wide zone in which the ocean properties are relaxed toward fixed temperature and salinity profiles on time scales varying linearly between 10 days (outermost cells) and 30 days (innermost cells) for the baroclinic solution and 1 and 2 h, respectively, for the barotropic solution. The conditions used for restoring are also used as the initial ocean properties everywhere in the domain. The chosen profiles include a well-mixed upper layer, a pycnocline, and weak salt stratification of the isothermal deep water, as illustrated in Fig. 3. These conditions are a reasonable generalization of the continental shelf waters surrounding most of Antarctica (Jacobs et al. 1985; Wong et al. 1998; Hellmer et al. 1998; Nicholls et al. 2003). Salinity variations have only a small influence on melt rates (see next section) so the salinity profile is fixed in all simulations to a 100-m-thick mixed layer of salinity 33.5, increasing to 34.5 at 200-m depth and 34.8 at the seabed. The ocean temperature is fixed to −1.8°C in the mixed layer (top 100 m) in all simulations and then changes linearly with depth toward the deep-water temperature, T_D, which is uniform from 200-m depth to the seabed. As illustrated in Fig. 3, the use of a constant deep-water temperature produces a thermal driving (the temperature above freezing actually involved in melting) that increases with depth as a result of the decrease in the freezing temperature. The temperature of water masses that may occupy Antarctica's shelf seas under plausible warming scenarios ranges from that of the coldest possible source water, HSSW at the surface freezing temperature (−1.8°C), to "core" CDW of a significantly warmer temperature than that currently found on the shelf (+2.0°C). For each simulation class the melt rate study is performed by varying T_D in 0.2°C steps between these values.

b. Melting formulation

The physics of melting and freezing at an ice shelf base are discussed at various points in this paper, so it is useful to introduce the topic here. Since we are primarily interested in melting, we neglect the complex role of frazil ice formation and deposition as beyond the scope of this study; instead we consider only melting and freezing occurring directly at the ice shelf base. No-slip conditions at the ice shelf base produce an oceanic boundary layer in which the flow speed grows with distance from the ice shelf until the flow is dynamically unaffected by the existence of the boundary. The rate of ice shelf melting or freezing is primarily determined by the transfer of heat and salt across this boundary layer, which is in turn governed by vertical heat and salt gradients and the level of turbulence, a function of the flow rate. Heat conduction within the ice shelf also plays a secondary role in controlling the melt rate (Holland and Jenkins 1999).

To calculate the basal melt rate m' (positive for melting), we formulate balances of heat and salt flux at the ice shelf–ocean boundary and link the two by constraining the interface to be at the local freezing temperature (Jenkins and Bombosch 1995):

$$c_0\gamma_T|\mathbf{u}|(T - T_b) = m'L + m'c_I(T_b - T_I), \quad (2)$$

$$\gamma_S|\mathbf{u}|(S - S_b) = m'S_b, \quad \text{and} \quad (3)$$

$$T_b = aS_b + b + cB, \quad (4)$$

where $c_0 = 3974$ J kg^{-1} °C^{-1} and $c_I = 2009$ J kg^{-1} °C^{-1} are the specific heat capacities of water and ice; $|\mathbf{u}|$, T, and S are the speed, temperature, and salinity of the oceanic mixed layer; T_b and S_b are the temperature and salinity of the ice–ocean interface; γ_T and γ_S are coefficients representing the transfer of heat and salt through the boundary layer; $L = 3.35 \times 10^5$ J kg^{-1} is the latent heat of ice fusion; $T_I = -25$°C is the core temperature of the ice shelf; and $a = -0.0573$°C,

$b = 0.0832°C$, and $c = 7.61 \times 10^{-4}$ °C m^{-1}. Note that the γ_T and γ_S used in this study are dimensionless and therefore differ from those used in many previous studies by a factor of $|\mathbf{u}|$.

Terms on the left-hand side of (2) and (3) represent transfer of heat and salt across the oceanographic boundary layer, and the (first) terms on the right-hand side represent latent heat consumed and the salination of meltwater released during the melting process. The third term in (2) is an approximation of heat conduction within the ice shelf according to Holland and Jenkins (1999); we assume that salt does not diffuse through the ice. As the conductive term is relatively small and γ_T is only very weakly dependent upon the Reynolds number, (2) implies that the melt rate is roughly proportional to the product of mixed layer speed and ocean–interface temperature difference; we shall return to this point later.

Various oceanographic observations in the vicinity of ice shelves show a freshening trend (Jacobs 2006), and ice shelves are melted by water masses with a range of different salinities, but in this study we do not examine the effect of salinity variation on melting because it is negligible compared to the influence of temperature variation. Holland and Jenkins (1999) show that for a moderate thermal driving of 1°C (which corresponds to the 4°C range of T_D examined in this study, as described below), the corresponding change of 5 in the salinity difference $S - S_b$ has a small impact on the melt rate. This finding is confirmed by laboratory experiments (Sammakia and Gebhart 1983). Since the change in $S - S_b$ due to plausible variations in the far-field salinity is much smaller than 5, we conclude that salinity variations of a reasonable size are unimportant to the melt rate overall.

4. Results of default warming experiment

In this section we consider the results of the simulations in class A, starting with an examination of two illustrative cases. Simulation $A_{-1.8}$ is our closest proxy for the conditions of the larger ice shelves (Ross and Filchner–Ronne), which interact with HSSW generated by sea ice growth offshore of the ice front at temperatures of around −1.8°C. In contrast, simulation $A_{+1.0}$ represents some smaller ice shelves whose cavities are flushed by warmer waters, such as those fringing the Amundsen and Bellingshausen Seas in West Antarctica, which are melted by CDW at temperatures as high as +1.0°C.

Figure 4a shows mixed layer velocity vectors and ice shelf melt rates for simulation $A_{-1.8}$. In this case there is an area of relatively rapid flow and vigorous melting near the grounding line of the ice shelf, but basal freezing predominates everywhere else. Freezing peaks in the Coriolis-generated boundary current rising on the western side of the ice shelf, in accordance with the results of Holland and Feltham (2006). Figure 4b shows that the mixed layer velocity drops in the freezing zone because entrainment of salt into the rising meltwater causes it to lose buoyancy until it has a similar density to the waters below. At that point, it "separates" from the ice shelf, slowly flowing horizontally out into the open ocean before dissipating into the isothermal waters offshore. It is interesting to note that the results of simulation $A_{-1.8}$ differ slightly from those of Holland and Jenkins (2001), who performed a similar study. We attribute our meltwater separation, higher melt rates, and swifter mixed layer flow to the greater thickness of the ice shelf used in this study. The deeper grounding line of our ice shelf (1000-m depth rather than 700 m) has a lower freezing temperature, so water restored to −1.8°C at the northern boundary has more heat available for melting at the depth of the grounding line (Fig. 3).

Simulation $A_{+1.0}$ has melt rates and mixed layer velocities an order of magnitude larger. The pattern of melting is similar, with the greatest melt rates near the grounding line, but the basal freezing is significantly reduced in both area and proportion of the melt rate. Despite this, we find that maximum freezing rates increase with ocean warming, as also found by Williams et al. (2002). Figures 4c and 4d show that in this case the mixed layer flows faster and is thinner because it does not separate from the ice shelf; instead the meltwater plume rises to the ocean surface and spreads out there, blending with the cold mixed layer prescribed on the northern boundary. The higher melt rates generated by the warmer deep waters produce a larger volume of fresh meltwater relative to the amount of saline water entrained into the mixed layer from below. This creates a larger density (salinity) difference between the ascending mixed layer and the deeper waters, increasing the buoyancy forcing on the mixed layer and thus accelerating the rising plume.

When we consider horizontally averaged ice shelf melt rates from the steady state of all of the class A simulations, shown in Fig. 5a, it becomes clear that the response of the melt rate to thermal forcing is remarkably well represented by a quadratic function of T_D. This quadratic dependence is best explained by considering how the melting and freezing represented by (2)–(4) changes as we vary the thermal forcing. Since ocean salinity restoring is the same in all simulations, as a first-order approximation we can ignore variations in

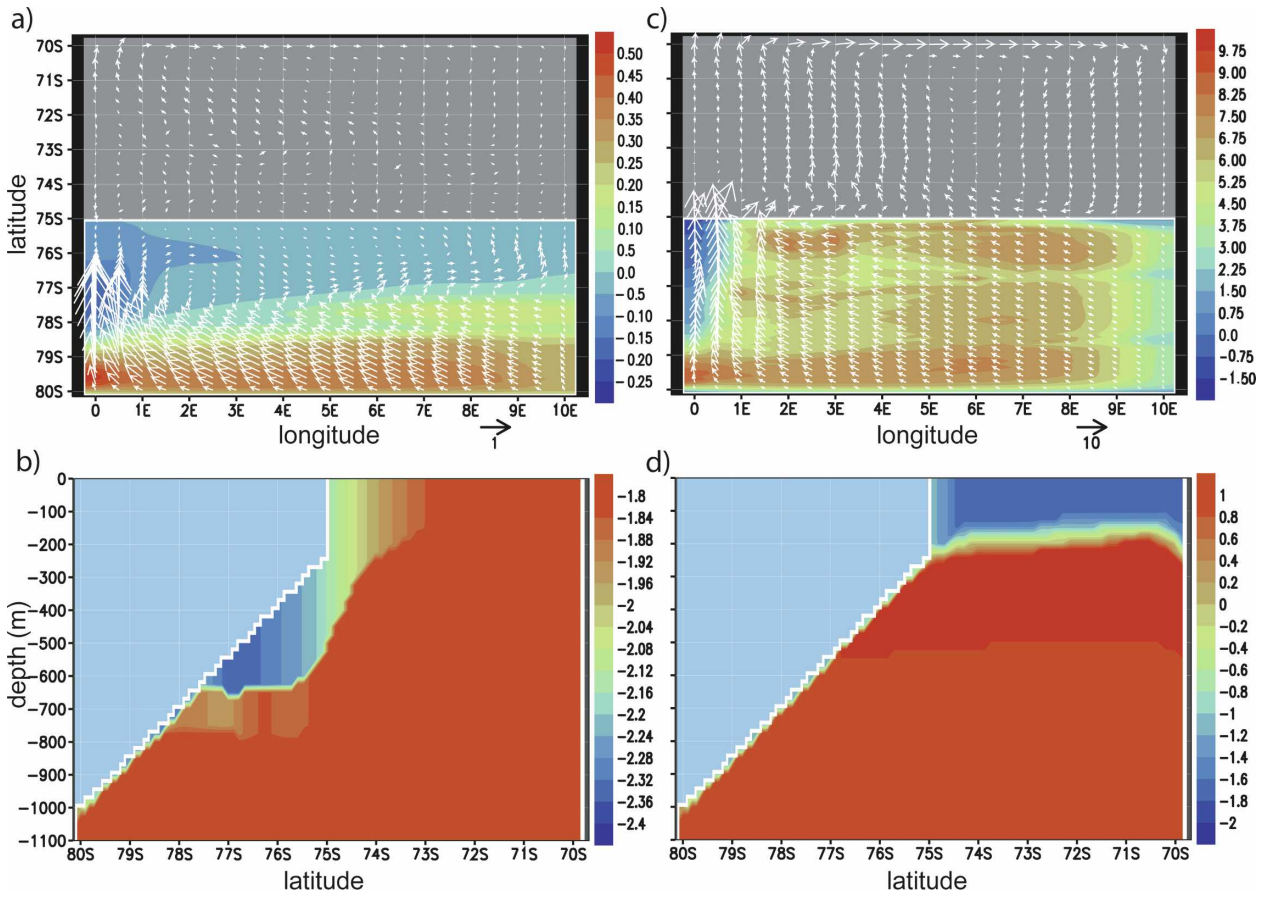

FIG. 4. Results of simulations (left) $A_{-1.8}$ and (right) $A_{+1.0}$: (a), (c) basal melt rate (m yr^{-1}, positive for melting) overlain by mixed layer velocity vectors (cm s^{-1}, plotted every grid point in longitude and every second grid point in latitude); (b), (d) longitudinal section of potential temperature (°C) along the center of the domain (5°E). Note the large differences in scale between plots. In (a) and (c) gray shading indicates the absence of the ice shelf and in (b) and (d) light blue shading indicates the ice shelf draft.

the salt flux balance and thus also ignore variations in the freezing temperature; this leaves us considering only (2). Conduction of heat within the ice shelf is roughly an order of magnitude smaller than heat transfer through the oceanic boundary layer, so if we now neglect the former and assume that γ_T is approximately constant, we find that m' is proportional to $|\mathbf{u}|(T - T_b)$. Figure 5b shows that the mixed layer velocity $\overline{|\mathbf{u}|}$ and ocean–interface temperature difference $\overline{T - T_b}$, averaged over the area covered by the ice shelf, are both linear functions of T_D and their product is therefore quadratic.

The fact that, despite this model's complexity, $\overline{T - T_b}$ and (particularly) $\overline{|\mathbf{u}|}$ rise linearly with an increase in the thermal forcing is a very interesting result. In a GCM such as this all variables are inextricably linked to each other, so an explanation of the variation in these model components requires examination of all. By considering a reduced system of equations representing the mixed layer beneath an ice shelf, we now attempt to explain the entire set of results shown in Fig. 5 and hence ultimately understand the quadratic nature of the melt rate variation. The reduced system is formulated by considering steady-state conditions in a rectangular section of the mixed layer in which ocean properties are constant in the same manner as within a model grid cell. From conservation equations for mass (mass flux divergence equals entrainment), momentum (a geostrophic balance between Coriolis acceleration and haline baroclinicity, the dominant component of the pressure gradient), heat (all heat entrained is used to melt the ice shelf), and salt (all salt entrained is used to salinate the fresh meltwater), we obtain

$$\nabla \cdot (D\mathbf{u}) = e', \tag{5}$$

$$f[-V, U] = g\beta(S - S_a)\nabla B, \tag{6}$$

$$Lm' = -c_0 e'(T - T_a), \quad \text{and} \tag{7}$$

$$m'S = -e'(S - S_a), \tag{8}$$

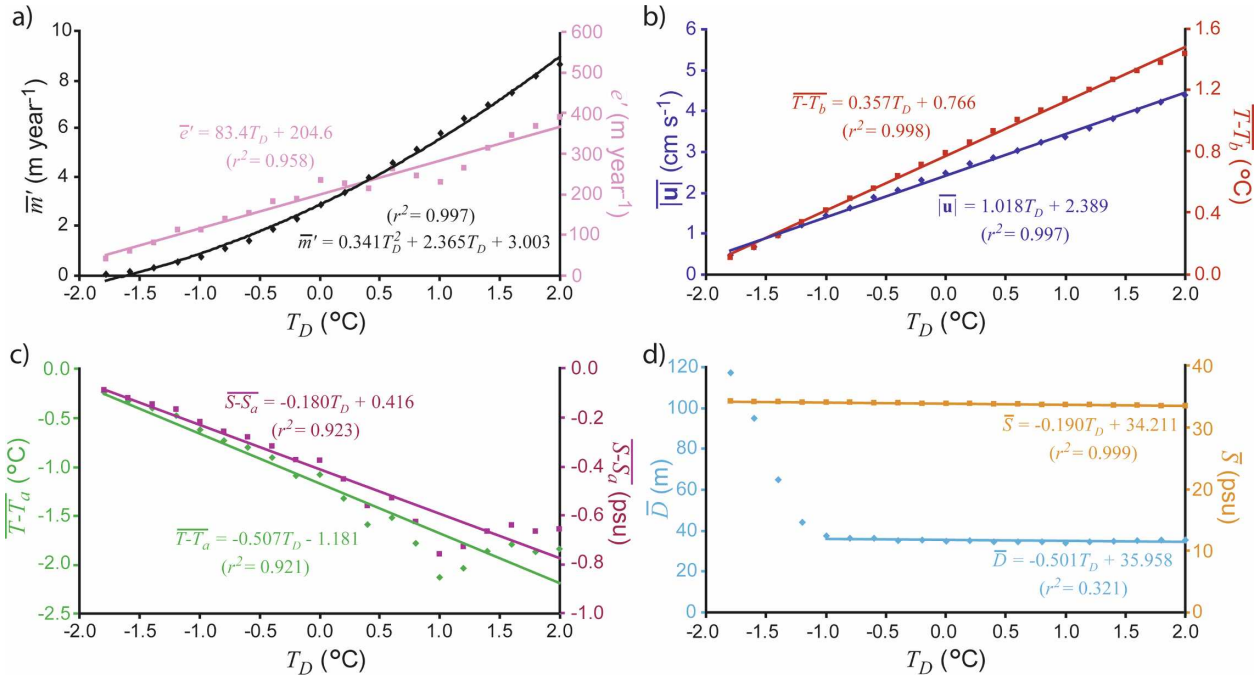

FIG. 5. The relations between mixed layer properties averaged over the area beneath the ice shelf and thermal forcing from all simulations in class A: (a) ice shelf melt rate and mixed layer entrainment rate, (b) mixed layer speed and mixed layer–interface temperature difference, (c) temperature and salinity differences between the mixed layer and its entrained water, and (d) mixed layer thickness and salinity.

where D and $\mathbf{u} = [U, V]$ are the mixed layer thickness and velocity, respectively, e' is the rate of entrainment into the mixed layer (positive for entrainment), $f = 1.4 \times 10^{-4}$ s^{-1} is the Coriolis parameter, $g = 9.81$ m s^{-2} is the gravitational acceleration, $\beta = \rho_0^{-1}\partial\rho/\partial S = 8 \times 10^{-4}$ is the haline contraction coefficient, and S_a and T_a are the salinity and temperature of the entrained seawater. In (6), ∇B is used as a proxy for the gradient of the interface between the mixed layer and the deep ocean on the basis that gradients in the mixed layer thickness are small. We now draw an analogy between this system, which is strictly applicable only to a single cell, and our model results averaged over the area beneath the ice shelf (denoted by overbars). The spatial patterns of D and $|\mathbf{u}|$ are similar throughout and almost identical over most of the temperature range ($T_D > -1$°C, after separation has ceased; Fig. 5d), so to simplify the discussion we use the variation of their spatially averaged values (Fig. 5) as a proxy for the variation in their spatial gradients, which appear in (5).

Our GCM and reduced system respond to variation in T_D as follows: as the deep ocean warms, the mixed layer velocity increases linearly (Fig. 5b), but its thickness remains approximately constant (Fig. 5d), so that the resulting linearly increased divergence is consistent with a linearly increasing entrainment (Fig. 5a) according to (5). Equation (6) states that the flow acceleration is caused by a linear rise in baroclinicity, associated with the steadily increasing salinity difference between the mixed layer and deep water (Fig. 5c) applied to a mixed layer that has a constant thickness pattern (Fig. 5d). According to (7), the quadratic increase in melt rate (Fig. 5a) is consistent with the product of the linear increases in both entrainment rate (Fig. 5a) and mixed layer–deep-water temperature difference (Fig. 5c). Finally, the variations in melt (quadratic) and entrainment (linear) rates and the mixed layer–deep-water salinity difference $S - S_a$ (linear) are all consistent according to the salt balance in (8) because $\overline{S}$ (Fig. 5c), which appears on the left-hand side of that equation, is approximately constant (unlike $\overline{S - S_a}$, its variation is a small proportion of its magnitude).

It is intriguing that the variation of these GCM results with respect to T_D can be encapsulated so well by a simplified system of equations, though it is not necessarily the case that the system will represent all subshelf ocean cavities. We demonstrate in the appendix that, subject to a few reasonable assumptions, a quadratic dependence of melt rate on temperature is a likely feature of this system and it follows that any de-

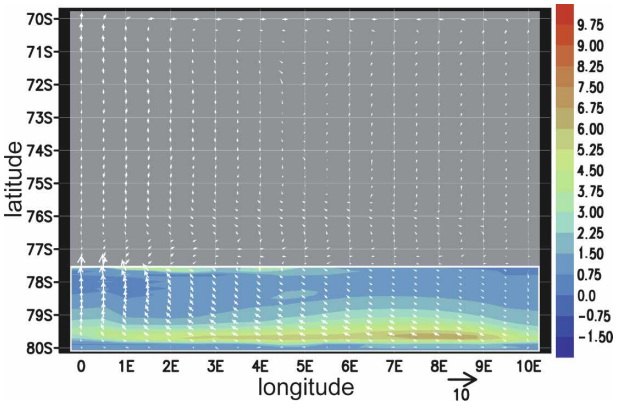

FIG. 6. Basal melt rate (m yr^{-1}) overlain by mixed layer velocity vectors (cm s^{-1}, plotted every grid point in longitude and every second grid point in latitude) in simulation $D_{+1.0}$. Scales are chosen to be the same as in Fig. 4c for comparative purposes. Gray shading indicates the absence of the ice shelf.

parture from the quadratic dependence described in this paper will require that additional behavior not described by (5)–(8) becomes significant.

5. Sensitivity to domain shape

In this section we examine the robustness of the quadratic melt rate–temperature relation to variation in the shape of the ice shelf cavity. To illustrate the range of results, we first consider simulation $D_{+1.0}$, in which a smaller, concave ice shelf profile is used in conjunction with northern-boundary restoring to relatively warm ocean properties (Fig. 6). Comparing these results to those of $A_{+1.0}$ (Fig. 4c) we find that melt rates beneath the nonlinear ice shelf are generally lower and melt is more focused around the steepest basal incline near the grounding line. No refreezing is predicted in this case. The general flow pattern is very similar to that of case $A_{+1.0}$, but the average flow speed is lower because the model only coarsely represents the steep southern part of the ice shelf base that should produce rapid flows. Since thermal forcing is similar in the two cases, this reduction in mixed layer flow is responsible for the drop in melt rates.

Figure 7 shows melt rates representative of all simulations performed in this study. All domain geometries feature a mean melt rate that depends upon T_D in the quadratic manner described in section 4, though we choose to only show the full response of simulation classes A–F to clarify the plot as much as possible. We find that ice shelves with a linear basal profile have a higher melt rate than those with a curved base and that smaller ice shelves have more vigorous melting than larger ones. In both cases this results from the model ice shelf base being represented as steeper on average. Walker and Holland (2007) also found that their melt rates decreased as the ice shelf base evolved from their near-linear initial slope into a more concave form. As the ocean is warmed, we find that the smaller, steeper ice shelves cease to support basal refreezing sooner (i.e., at a lower deep-water temperature) than the larger ice shelves. This agrees with observation in the sense that the refreezing of case $A_{+1.0}$ is not found under the smaller ice shelves in the Amundsen Sea (Jacobs et al. 1996). Figure 7 also shows that tapering the sidewalls decreases the average melt rate in proportion to the reduced area of melting near the grounding line, but changing the bedrock slope has virtually no effect upon the melt rate.

For comparison with the data of Rignot and Jacobs (2002), who only consider melting near the grounding line, we also studied the melt rate averaged only over the southernmost 0.5° of latitude (≈50 km) rather than the whole ice shelf. These averages also adhere to a quadratic relation with deep-water temperature. Plotted in Fig. 7 are results from cases $A_{+2.0}$ and $C_{+2.0}$, showing that this limited-area averaging produces a

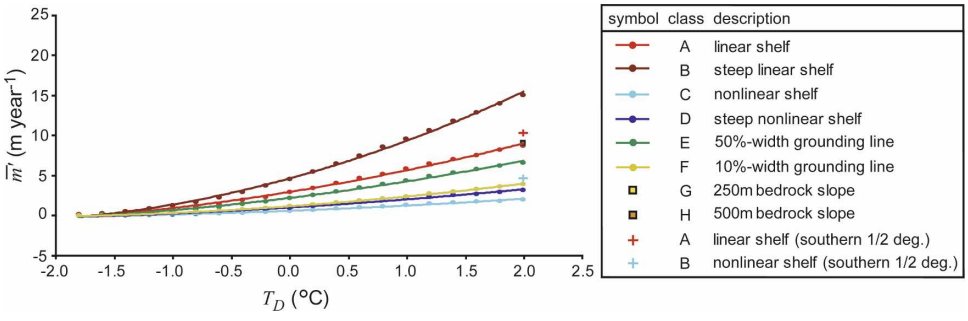

FIG. 7. The relation between mean melt rate and thermal forcing for all simulation classes used in this study. Curves drawn are quadratic fits to the results of classes A–F; the results of all classes exhibit quadratic behavior.

higher melt rate than taking the average for the whole ice shelf; the difference is particularly marked in case $C_{+2.0}$ because the nonlinear ice shelf profile significantly increases melt near the grounding line relative to the average. We therefore attribute the fact that our results show generally lower melt rates than those of previous studies (Fig. 1) to two things: first, our ice shelves have larger, shallower profiles than those that in reality produce the highest melt rates, and second, we plot the average melt rate over the whole ice shelf rather than only that near the grounding line.

6. Discussion

We have shown that the ice shelf basal melting predicted by our full GCM responds to ocean warming in a quadratic fashion, and that all model results can be described using a reduced system of equations. With a few additional assumptions, we show that the applicability of the reduced system implies this quadratic response (see the appendix). We now discuss the limitations of the model used here before comparing our results to those of the previous studies described in section 2.

It seems likely that the melting formulation (2)–(4) is of critical importance to our quadratic relation because it sets the melt rate to be proportional to the product of mixed layer velocity and mixed layer–interface temperature difference. Other studies use a simplified melting formulation that is only proportional to temperature difference (Williams et al. 1998, 2001; Timmermann et al. 2002), which could lead to rather different behavior (although it is conceivable that other factors could compensate to restore the nonlinearity). The use of more complex melting parameterizations than (2)–(4) could be envisaged, but none could drastically change the basic proportionality between melting and the product of ocean speed and temperature (Holland and Jenkins 1999). Our finding that the mixed layer velocity and ocean–ice temperature difference both rise linearly with ocean warming is not trivial, and it is particularly interesting that the gradient of increase in $\overline{T - T_b}$ is 0.36 (Fig. 5b). This implies that the temperature difference driving steady-state ice shelf melting is increased by approximately one-third of the temperature increase applied at the northern boundary. A closer examination of the results reveals that this occurs because a mixed layer temperature rise of 49% of the T_D increase is offset by a 13% (of the T_D increase) rise in the ice shelf–ocean interface temperature T_b (increased melting lowers S_b and thus raises T_b).

The modeling approach used in this study has both advantages and disadvantages. For example, using an ocean GCM is computationally expensive but allows us to scrutinize the behavior of the full equations of motion. Using a simplified domain generalizes the results, but raises the possibility that our conclusions might not be applicable to complex real-world domains, though we have shown that our idealized cases qualitatively reproduce the behavior of both large ice shelves forced by cold shelf waters and smaller ice shelves forced by warmer deep waters. The use of an idealized scenario also helps to avoid confusion about what temperature we are varying to examine the melt rate response. In previous studies, authors have considered variation with respect to temperatures located offshore of, at, and shoreward of the ice front. Similarly, depth-uniform temperatures and those taken from real profiles (either pointwise or depth averaged) have been considered. How the varied temperature relates to thermal driving is in reality a function of the depth of the ice shelf (considering the freezing temperature's decrease with depth; Fig. 3), the position of that temperature with respect to the ice front, and the ocean dynamics within the cavity.

The GCM used in this study has a few important simplifications that are worthy of comment. We have neglected the influence of tides in the model, but since this will not significantly change with ocean warming, we feel that this is justified as long as buoyancy still controls ocean flow. If tides were to dominate, the rise in mixed layer velocity could be unimportant, and the melt rate would then rise linearly overall. Another important omission is that of sea ice formation in the continental shelf seas offshore of the ice front. The basal melt rates of the largest ice shelves follow an annual cycle because the waters flushing the ice shelf cavity are formed from the brine rejected during sea ice formation, which peaks in winter (Jenkins et al. 2004). The resulting salinity variation is of negligible direct importance to the melting, but the effect of variation in the cavity flushing time scale on the overall heat flux into the cavity is significant and not modeled here. We might expect a stronger influence of bedrock slope than found in Fig. 7 if the circulation were dominated by dense-water formation offshore of the ice front.

It is interesting to note that a nonlinear melt rate response is also reported by Jenkins (1991) and found in test versions of the Jenkins and Bombosch (1995) and Holland and Feltham (2006) plume models, despite the greater simplicity of their approaches. The basic concept of these models is that a vertically well-mixed plume lies between the ice shelf and the stratified ambient fluid, so they are similar in approach to our mixed layer parameterization, albeit with fixed deep-water properties in place of our varying isopycnic layers. The

fact that our model qualitatively agrees with these results implies that virtually all extra heat from the offshore warming is transported into the ice shelf cavity. Our results also agree with those of Hellmer et al. (1998), so from an ocean-warming perspective their model can be viewed as a zonally averaged version of our own.

Agreeing with the quadratic relations found by these models does not necessarily mean that we must disagree with the power laws determined in experimental studies, which all have exponents less than two (Greisman 1979; Russell-Head 1980; Josberger and Martin 1981). There is a difference between fitting a quadratic function, where the constants multiplying a series of terms are varied to produce the best fit, and fitting a power law, where the constant and power of a single term are varied. If we fit a power law to our model results we obtain an exponent of 1.61 ($r^2 = 0.994$), so the linear and constant terms in our quadratic act to reduce the nonlinearity when the response is viewed in this way. It is quite fascinating that by spatially averaging our model results, which incorporate the detail of large-scale ocean flow beneath ice shelves, we find a similar functional response to warming to that determined by experimental studies of ice melting on scales of tens of centimeters.

The above discussion implies that our results do not agree with the square power law arising from the theory proposed by MacAyeal (1984). There are several reasons why our model would have a more moderate response to warming; probably the most important is that $|\mathbf{u}|$ and $T - T_b$ decrease linearly with ocean cooling but do not tend to zero as T_D approaches -1.8°C, because at depth this temperature still implies a nonzero thermal driving (Fig. 3). As linear functions of T_D, both quantities thus have an intercept (Fig. 5b), and their product is a quadratic function with significant linear and constant terms. The velocity and melt rate of MacAyeal (1984) are both single-term linear functions of the temperature above the freezing point, so their product is strictly a square power law. In addition, our melting parameterization incorporates conduction of heat into the ice shelf, which has a moderating effect on the melt rate.

The roughly linear relationships between melt rate and ocean temperature found by Grosfeld and Sandhäger (2004) and Payne et al. (2007) are not overtly in disagreement with our results because the temperature ranges that they investigate are relatively small (Fig. 1). However, if our findings are correct, the larger temperature range scrutinized by Williams et al. (2002) should produce some nonlinearity in their results. We attribute the linearity of their results primarily to their maintenance of a constant barotropic exchange at the ice front, which fundamentally controls the heat flux into the cavity. In our simulations, warming of the deep waters at the northern boundary increases velocities and temperatures everywhere in the domain linearly, producing a quadratically increased heat flux into the ice shelf cavity. In the Williams et al. (2002) simulations the water at the ice front warms, but its velocity is fixed, leading to a linear increase in the heat flux into the cavity and therefore linearly increasing the melt rate.

The quadratic relation found in this study may appear to disagree fundamentally with the linear fits plotted by Rignot and Jacobs (2002) and Shepherd et al. (2004) because we find that the melt rate is quadratically related to deep ocean temperature even when only a narrow region near the grounding line is considered. However, it should be noted that the studies are not directly comparable because temperature is the only quantity varied to produce our quadratic relations while variations in ice shelf topography, ocean forcing, etc., occur between observations in the satellite studies, which could account for the scatter between data points (Fig. 1). It might be the case that the differences between individual ice shelves average out to produce a linear relation overall, but the effect of warming on any one particular ice shelf is nonlinear.

7. Conclusions

By applying a full ocean general circulation model to idealized ice shelf cavities, we have determined that the response of ice shelf basal melting to ocean warming follows a quadratic relation. This occurs because the melt rate is primarily governed by the transfer of heat through the oceanic boundary layer beneath the ice shelf, which is influenced by changes in both oceanic temperature and velocity. As the ocean warms offshore of an ice shelf, both of these quantities increase linearly, leading to a quadratic increase overall. Examination of a range of model configurations shows that altering topography changes the magnitude of the melt rate, but not the quadratic response to warming.

This result agrees closely with earlier experimental and idealized modeling work, but is inconsistent with other studies, notably some detailed models and satellite observation. This modeling study is the first to attempt to study the response of ice shelves to warming over the entire range of relevant temperatures, applying a relatively full formulation of both ice shelf melting and general ocean physics to idealized topographies. A major advantage of this approach is that the ocean tem-

perature to be varied is a well-defined quantity (the deep-water temperature on the continental shelf some distance offshore of the ice front). The study acts as a proxy for examining either variation in the melting of a single ice shelf as the ocean warms or the difference in melt rates between topographically similar ice shelves that experience different oceanographic forcings.

It is important to note that we make no claims about the source of the hypothesized warming. Several studies have proposed that oceanic warming has triggered increased mass loss from the grounded Antarctic ice sheet (e.g., Shepherd et al. 2004), but no persistent warming (of waters actually melting an ice shelf) has yet been measured. Warm waters that penetrate ice shelf cavities upwell from great depths and might not be directly impacted by atmospheric warming on short time scales. One explanation for oceanic temperature changes is that a change in circulation alters the flow of existing warm water masses onto the continental shelf, as a result of variation in the southern annular mode, for example (Jacobs 2006). The only assumption made in this study is that a change occurs in the deep-water temperature on the continental shelf.

Our finding of a nonlinear relation between melt rate and ocean temperature contradicts some established ideas. Several authors and the 2007 Intergovernmental Panel on Climate Change report (Lemke et al. 2007) suggest that a single melt rate–temperature sensitivity (in m yr^{-1} $°C^{-1}$) is applicable to all ice shelves and temperatures, but our results imply that this is inaccurate in general. Instead, each ice shelf has a nonlinear melt–temperature curve, so that the melt rate sensitivity varies with both topography and temperature. The relations we find could certainly be approximated as linear over the small temperature ranges of relevance to the medium-term future of individual ice shelves, but a single linear relation cannot be true for all ice shelves. Our central result also disagrees with the Beckmann and Goosse (2003) parameterization of ice shelf melting, since they do not consider the important impact of variation in the sub–ice shelf velocity and therefore derive a linear relation between melt rate and ocean temperature (the model results that their parameterization is based on had melt rate solely as a function of ocean temperature).

The quadratic melt rate dependence should be of interest to scientists concerned about the long-term effects of global warming on Antarctic climate stability as a whole. First, it implies that for a given topography, ice shelves melted by warm waters are more sensitive to temperature changes. Second, if a steady warming of waters offshore of an ice shelf were to take place, then our results imply that melting of the ice shelf base would increase at an accelerating rate. Whether this leads to thinning or collapse of the ice shelf will also depend upon glaciological and meteorological processes, but the fact that the melting increase accelerates requires that some other process counteracts melting in an above-linear fashion to stabilize the ice shelf and, therefore, the ice sheet feeding it.

Acknowledgments. DMH acknowledges support from the United States National Science Foundation Grants OPP-0327664, OPP-0337073, and OCE-0350912.

APPENDIX

Response of an Idealized Sub–Ice Shelf Mixed Layer to Ocean Warming

This appendix aims to show that the simplified mixed layer represented by (5)–(8) generally produces a quadratic relation between melt rate and deep ocean temperature T_D. Our goal is to understand how this system changes as T_D varies, so we rewrite the system using "script" font characters to define variables representing the quantities that vary with respect to T_D: $\mathcal{D} = D$, $\mathcal{E} = e'$, $\mathcal{F} = S$, $\mathcal{M} = m'$, $\mathcal{S} = S - S_a$, $\mathcal{T} = T - T_a$, and $\mathcal{U} = U$. We also simplify the analysis by rotating the coordinate axes until the x direction is aligned with the flow and then integrating over the area of the cell, leading to

$$\mathcal{D}\mathcal{U} = \Delta x \mathcal{E} + C_1, \tag{A1}$$

$$f \Delta y \mathcal{U} = g\beta B \mathcal{S} + C_2, \tag{A2}$$

$$L\mathcal{M} = -c_0 \mathcal{E}\mathcal{T}, \quad \text{and} \tag{A3}$$

$$\mathcal{M}\mathcal{F} = -\mathcal{E}\mathcal{S}, \tag{A4}$$

where C_1, C_2 are constants.

We now argue that the change in each quantity with respect to T_D (here denoted by a subscript T) takes the form of a polynomial, and our aim then becomes to determine the powers of T_D in the polynomial's significant terms. For example, if we state that $\mathcal{M}_T = \sum_{i=1}^{\infty} c_i T_D^i$, where, c_i are constants, we wish to know the power m associated with the highest-order significant term in $\mathcal{M}_T$. Assuming that all lower-order terms are also important, we are then making the approximation $\mathcal{M}_T \approx \sum_{i=1}^{m} c_i T_D^i$. However, the aim of this appendix is to determine only the power associated with the highest-order significant term of each variable, so we restrict our attention to the system when, for example, $\mathcal{M}_T \approx c_m T_D^m$. Substituting similar expressions into our system of equations, we obtain:

$$c_d c_u T_D^{d+u} = \Delta x c_e T_D^e + C_1, \quad \text{(A5)}$$

$$f \Delta y c_u T_D^u = g\beta B c_s T_D^s + C_2, \quad \text{(A6)}$$

$$L c_m T_D^m = -c_0 c_e c_t T_D^{e+t}, \quad \text{and} \quad \text{(A7)}$$

$$c_m c_f T_D^{m+f} = -c_e c_s T_D^{e+s}. \quad \text{(A8)}$$

Using dimensional analysis on T_D, this leads to the following:

$$d + u = e, \quad \text{(A9)}$$

$$u = s, \quad \text{(A10)}$$

$$m = e + t, \quad \text{and} \quad \text{(A11)}$$

$$m + f = e + s. \quad \text{(A12)}$$

We have now transformed our original system into a set of equations describing how the quantities involved vary in relation to each other. However, we require additional assumptions to close the system. If we assume that varying T_D has very little effect on S (see section 4 and Fig. 5d), then $f = 0$. If we also assume that entrainment behaves according to the simple relation of Pederson (1980),

$$e' = E_0 U \sin\theta, \quad \text{(A13)}$$

where E_0 is the entrainment coefficient and θ is the angle of the ice shelf base with respect to horizontal, then by following the procedure above we may infer that $e = u$ and this, combined with (A9), implies that $d = 0$. This agrees with the results of our model (Fig. 5d).

Setting $d = f = 0$ in (A9)–(A12), it may easily be deduced that $m = 2t$, so we know that m' varies according to a relation with twice the power of the variation in $T - T_a$. If we now neglect the conductive term in (2), we find that the diffusive heat transfer in that equation equals the latent heat release or uptake, and after substituting this and the entrainment parameterization (A13) into (7), we arrive at

$$\gamma_T (T - T_b) = -E_0 \sin\theta (T - T_a) \quad \text{(A14)}$$

and rearranging we find that

$$T - T_a = \frac{\gamma T (T_b + T_a)}{\gamma_T - E_0 \sin\theta}. \quad \text{(A15)}$$

Since T_b is relatively constant as T_D varies [T_b increases by approximately 10% of T_D because S_b decreases; see (4)], we have shown that $T - T_a$ varies in a similar fashion to T_a, which in turn behaves almost identically to T_D. Therefore, $T - T_a$ can be related linearly to T_D and $t = 1$, implying that $m = 2$ and the melt rate is a quadratic function of deep-water temperature.

The extra assumptions outlined above are reasonable and all found to be true in this study (Fig. 5) and also in test versions of the Jenkins and Bombosch (1995) and Holland and Feltham (2006) plume models. The applicability of the reduced system (5)–(8) therefore implies that the melt rate is likely to increase quadratically with changes in ocean temperature.

REFERENCES

Beckmann, A., and H. Goosse, 2003: A parameterization of ice shelf–ocean interaction for climate models. *Ocean Modell.,* **5,** 157–170.

Budd, W. F., T. H. Jacka, and V. I. Morgan, 1980: Antarctic iceberg melt rates derived from size distributions and movement rates. *Ann. Glaciol.,* **9,** 103–112.

Gade, H. G., 1993: When ice melts in sea water: A review. *Atmos.–Ocean,* **31,** 139–165.

Gebhart, B., B. Sammakia, and T. Audunson, 1983: Melting characteristics of horizontal ice surfaces in cold saline water. *J. Geophys. Res.,* **88,** 2935–2942.

Gille, S. T., 2002: Warming of the Southern Ocean since the 1950s. *Science,* **295,** 1275–1277.

Giulivi, C. F., and S. S. Jacobs, 1997: Oceanographic data in the Amundsen and Bellingshausen Seas: N.B. Palmer cruise 9402, February–March 1994. Lamont-Doherty Earth Observatory Tech. Rep. 97-3, 330 pp.

Greisman, P., 1979: On upwelling driven by the melt of ice shelves and tidewater glaciers. *Deep-Sea Res. I,* **26,** 1051–1065.

Grosfeld, K., and R. Gerdes, 1998: Circulation beneath the Filchner Ice Shelf, Antarctica, and its sensitivity to changes in the oceanic environment: A case study. *Ann. Glaciol.,* **27,** 99–104.

——, and H. Sandhäger, 2004: The evolution of a coupled ice shelf–ocean system under different climate states. *Global Planet. Change,* **42,** 107–132.

Hamley, T. C., and W. F. Budd, 1986: Antarctic iceberg distribution and dissolution. *J. Glaciol.,* **32,** 242–251.

Hellmer, H. H., and S. S. Jacobs, 1995: Seasonal circulation under the eastern Ross Ice Shelf, Antarctica. *J. Geophys. Res.,* **100,** 10 873–10 885.

——, ——, and A. Jenkins, 1998: Oceanic erosion of a floating Antarctic glacier in the Amundsen Sea. *Ocean, Ice, and Atmosphere: Interactions at the Antarctic Continental Margin,* S. S. Jacobs and R. F. Weiss, Eds., Antarctic Research Series, Vol. 75, Amer. Geophys. Union, 83–99.

Holland, D. M., and A. Jenkins, 1999: Modeling thermodynamic ice–ocean interactions at the base of an ice shelf. *J. Phys. Oceanogr.,* **29,** 1787–1800.

——, and ——, 2001: Adaptation of an isopycnic coordinate ocean model for the study of circulation beneath ice shelves. *Mon. Wea. Rev.,* **129,** 1905–1927.

Holland, P. R., and D. L. Feltham, 2006: The effects of rotation and ice shelf topography on frazil-laden ice shelf water plumes. *J. Phys. Oceanogr.,* **36,** 2312–2327.

Jacobs, S. S., 2006: Observations of change in the Southern Ocean. *Philos. Trans. Roy. Soc. London,* **A364,** 1657–1681.

——, R. G. Fairbanks, and Y. Horibe, 1985: Origin and evolution of water masses near the Antarctic continental margin: Evidence from $H_2^{18}O/H_2^{16}O$ ratios in seawater. *Oceanology of the Antarctic Continental Shelf,* S. S. Jacobs, Ed., Antarctic Research Series, Vol. 43, Amer. Geophys. Union, 59–85.

——, H. H. Hellmer, C. S. M. Doake, A. Jenkins, and R. M. Frolich, 1992: Melting of ice shelves and the mass balance of Antarctica. *J. Glaciol.,* **38,** 375–387.

——, ——, and A. Jenkins, 1996: Antarctic Ice Sheet melting in the Southeast Pacific. *Geophys. Res. Lett.,* **23,** 957–960.

Jenkins, A., 1991: Ice shelf basal melting: Implications of a simple mathematical model. FRISP Rep. 5, 32–36.

——, and A. Bombosch, 1995: Modeling the effects of frazil ice crystals on the dynamics and thermodynamics of Ice Shelf Water plumes. *J. Geophys. Res.,* **100,** 6967–6981.

——, D. M. Holland, K. W. Nicholls, M. Schröder, and S. Østerhus, 2004: Seasonal ventilation of the cavity beneath Filchner-Ronne Ice Shelf simulated with an isopycnic coordinate ocean model. *J. Geophys. Res.,* **109,** C01024, doi:10.1029/2001JC001086.

——, H. F. J. Corr, K. W. Nicholls, C. L. Stewart, and C. S. M. Doake, 2006: Interactions between ice and ocean observed with phase-sensitive radar near an Antarctic ice-shelf grounding line. *J. Glaciol.,* **52,** 325–346.

Josberger, E. G., and S. Martin, 1981: A laboratory and theoretical study of the boundary layer adjacent to a vertical melting ice wall in salt water. *J. Fluid Mech.,* **111,** 439–473.

Joughin, I., E. J. Rignot, C. E. Rosanova, B. K. Luccitta, and J. Bohlander, 2003: Timing of recent accelerations of Pine Island Glacier, Antarctica. *Geophys. Res. Lett.,* **30,** 1706, doi:10.1029/2003GL017609.

Lemke, P., and Coauthors, 2007: Observations: Changes in snow, ice and frozen ground. *Climate Change 2007: The Physical Science Basis,* S. Solomon et al., Eds., Cambridge University Press, 338–383.

Levitus, S., J. I. Antonov, T. P. Boyer, and C. Stephens, 2000: Warming of the world ocean. *Science,* **287,** 2225–2229.

——, ——, and ——, 2005: Warming of the world ocean, 1955–2003. *Geophys. Res. Lett.,* **32,** L02604, doi:10.1029/2004GL021592.

MacAyeal, D. R., 1984: Thermohaline circulation below the Ross Ice Shelf: A consequence of tidally induced vertical mixing and basal melting. *J. Geophys. Res.,* **89,** 597–606.

Marshall, G. J., P. A. Stott, J. Turner, W. M. Connolley, J. C. King, and T. A. Lachlan-Cope, 2004: Causes of exceptional atmospheric circulation changes in the Southern Hemisphere. *Geophys. Res. Lett.,* **31,** L14205, doi:10.1029/2004GL019952.

Nicholls, K. W., and S. Østerhus, 2004: Interannual variability and ventilation timescales in the ocean cavity beneath Filchner-Ronne Ice Shelf, Antarctica. *J. Geophys. Res.,* **109,** C04014, doi:10.1029/2003JC002149.

——, L. Padman, M. Schröder, R. A. Woodgate, A. Jenkins, and S. Østerhus, 2003: Water mass modification over the continental shelf north of Ronne Ice Shelf, Antarctica. *J. Geophys. Res.,* **108,** 3260, doi:10.1029/2002JC001713.

Orsi, A. H., G. C. Johnson, and J. L. Bullister, 1999: Circulation, mixing, and production of Antarctic Bottom Water. *Prog. Oceanogr.,* **43,** 55–109.

Payne, A. J., P. R. Holland, A. P. Shepherd, I. C. Rutt, A. Jenkins, and I. Joughin, 2007: Numerical modeling of ocean–ice interactions under Pine Island Bay's ice shelf. *J. Geophys. Res.,* **112,** C10019, doi:10.1029/2006JC003733.

Pederson, F. B., 1980: Dense bottom currents in rotating ocean. *J. Hydraul. Div. Amer. Soc. Civ. Eng.,* **106,** 1291–1308.

Rignot, E. J., 1998: Fast recession of a West Antarctic glacier. *Science,* **281,** 549–551.

——, and S. S. Jacobs, 2002: Rapid bottom melting widespread near Antarctic Ice Sheet grounding lines. *Science,* **296,** 2020–2023.

——, and R. H. Thomas, 2002: Mass balance of polar ice sheets. *Science,* **297,** 1502–1506.

——, G. Casassa, P. Gogineni, W. Krabill, A. Rivera, and R. Thomas, 2004: Accelerated ice discharge from the Antarctic Peninsula following the collapse of Larsen B Ice Shelf. *Geophys. Res. Lett.,* **31,** L18401, doi:10.1029/2004GL020697.

Russell-Head, D. S., 1980: The melting of free-drifting icebergs. *Ann. Glaciol.*, **9,** 119–122.

Sammakia, B., and B. Gebhart, 1983: Transport near a vertical ice surface melting in water of various salinity levels. *Int. J. Heat Mass Transfer,* **26,** 1439–1452.

Scambos, T. A., C. Hulbe, M. Fahnestock, and J. Bohlander, 2000: The link between climate warming and break-up of ice shelves in the Antarctic Peninsula. *J. Glaciol.,* **46,** 516–530.

Shepherd, A. P., D. J. Wingham, and E. J. Rignot, 2004: Warm ocean is eroding West Antarctic Ice Sheet. *Geophys. Res. Lett.,* **31,** L23402, doi:10.1029/2004GL021106.

Smedsrud, L. H., and A. Jenkins, 2004: Frazil ice formation in an Ice Shelf Water plume. *J. Geophys. Res.,* **109,** C03025, doi:10.1029/2003JC001851.

Timmermann, R., H. H. Hellmer, and A. Beckmann, 2002: Simulations of ice–ocean dynamics in the Weddell Sea 2. Interannual variability 1985–1993. *J. Geophys. Res.,* **107,** 3025, doi:10.1029/2000JC000742.

Van der Veen, C. J., 1999: *Fundamentals of Glacier Dynamics.* Balkema, 462 pp.

Walker, R. T., and D. M. Holland, 2007: A two-dimensional coupled model for ice shelf–ocean interaction. *Ocean Modell.,* **17,** 123–139.

Williams, M. J. M., R. C. Warner, and W. F. Budd, 1998: The effects of ocean warming on melting and ocean circulation under the Amery Ice Shelf, East Antarctica. *Ann. Glaciol.,* **27,** 75–80.

——, K. Grosfeld, R. C. Warner, R. Gerdes, and J. Determann, 2001: Ocean circulation and ice–ocean interaction beneath the Amery Ice Shelf, Antarctica. *J. Geophys. Res.,* **106,** 22 383–22 399.

——, R. C. Warner, and W. F. Budd, 2002: Sensitivity of the Amery Ice Shelf, Antarctica, to changes in the climate of the Southern Ocean. *J. Climate,* **15,** 2740–2757.

Wingham, D. J., A. Shepherd, A. Muir, and G. J. Marshall, 2006: Mass balance of the Antarctic Ice Sheet. *Philos. Trans. Roy. Soc. London,* **A364,** 1627–1635, doi:10.1098/rsta.2006.1792.

Wong, A. P. S., N. L. Bindoff, and A. Forbes, 1998: Ocean–ice shelf interaction and possible bottom water formation in Prydz Bay, Antarctica. *Ocean, Ice, and Atmosphere: Interactions at the Antarctic Continental Margin,* S. S. Jacobs and R. F. Weiss, Eds., Antarctic Research Series, Vol. 75, Amer. Geophys. Union, 173–187.

Zwally, H. J., M. B. Giovinetto, J. Li, H. G. Cornejo, M. A. Beckley, A. C. Brenner, J. L. Saba, and D. Yi, 2005: Mass changes of the Greenland and Antarctic ice sheets and shelves and contributions to sea-level rise: 1992–2002. *J. Glaciol.,* **51,** 509–527.